Wavelet Transform-Based Interferometric SAR Coherence Estimator

C. López-Martínez, *Member, IEEE*, X. Fàbregas, *Member, IEEE*, and E. Pottier, *Member, IEEE*

***Abstract*—A novel method to estimate interferometric coherence in synthetic aperture radar interferometry is proposed. It is demonstrated that this approach is not affected by the terrain topography, contrary to multilook techniques. In addition, since the method is based on the two-dimensional discrete wavelet packet transform, it allows recovering coherence information with a high spatial resolution. Results derived from simulated and experimental ESAR-DLR X- and L-band interferograms corroborate the performance of the proposed technique.**

***Index Terms*—Coherence, discrete wavelet transform (DWT), interferometry, synthetic aperture radar (SAR).**

I. Introduction

SYNTHETIC aperture radar (SAR) interferometry (InSAR) is able to retrieve the terrain topography from complex interferograms [1]. An interferogram consists of the complex Hermitian product of two SAR images acquired from slightly different spatial locations. Consequently, the complex Hermitian product phase contains topographic information coded in a 2π modulus, which must be unwrapped to derive height information unambiguously.

The correlation coefficient of a pair of SAR images S_1 and S_2 is an important source of information [2]

$$\rho = |\rho| \exp(j\phi_x) = \frac{E\{S_1 S_2^*\}}{\sqrt{E\{|S_1|^2\}E\{|S_2|^2\}}} \tag{1}$$

where $E\{x\}$ is the ensemble average and * is the complex conjugate. The amplitude of (1), i.e., $|\rho|$, called coherence, determines the precision of the derived topographic information. Coherence is also important since it may be employed in the phase unwrapping process or to estimate the signal-to-noise ratio of the SAR system. In combination with polarimetric techniques, coherence can be also employed to derive forest height [3]. Coherence depends on many factors, for instance, the signal-to-noise ratio of the SAR system, the co-registration process of the SAR images, or the so-called temporal decorrelation term, which accounts for coherence losses when SAR images are acquired at different times. Finally, the spatial or geometric decorrelation takes into account the fact that both SAR images do not observe exactly the same area, since they are acquired from different spatial locations [4]. Since SAR images cover from tens to hundreds of kilometers, with spatial resolutions from meters to tens of meters, coherence must be estimated locally since all the previous factors are nonhomogeneous in the SAR images.

Under the assumption that S_1, S_2, and $S_1 S_2^*$ are homogeneous and ergodic in mean, (1) may be estimated locally by means of the multilook coherence estimator

$$|\rho_{\mathrm{MLT}}| = \frac{\left|\sum_{m=1}^{M}\sum_{n=1}^{N} S_1(m,n)S_2^*(m,n)\right|}{\sqrt{\sum_{m=1}^{M}\sum_{n=1}^{N}|S_1(m,n)|^2 \sum_{m=1}^{M}\sum_{n=1}^{N}|S_2(m,n)|^2}} \tag{2}$$

where m and n are the spatial coordinates. Equation (2) overestimates low coherences in such a way that the larger the number of averaged pixels, the lower the coherence bias [2], but also, the larger the loss of spatial resolution and spatial details [5]. In the case of InSAR, even if S_1 and S_2 are homogeneous, they can differ in a deterministic and nonhomogeneous phase component ϕ_x, representing the topographic induced phase [2], [6]. If ϕ_x is constant within the $m \times n$ analysis window, it does not affect coherence estimation. Nevertheless, if ϕ_x is not constant, it induces a second bias term into the multilook estimator (2). Thus, it is necessary to compensate ϕ_x in order to estimate unbiased coherence values. The estimator bias is especially problematic for mountainous areas, where ϕ_x presents a large variability due to steep slopes. The topography compensated coherence estimator [6] is shown in

$$|\rho_{\mathrm{PHC}}| = \frac{\left|\sum_{m=1}^{M}\sum_{n=1}^{N} S_1(m,n)S_2^*(m,n)\exp(-j\hat{\phi}_x(m,n))\right|}{\sqrt{\sum_{m=1}^{M}\sum_{n=1}^{N}|S_1(m,n)|^2 \sum_{m=1}^{M}\sum_{n=1}^{N}|S_2(m,n)|^2}} \tag{3}$$

where $\hat{\phi}_x$ is the estimated topographic component. The phase component ϕ_x can be obtained by means of external digital elevation models (DEMs), or it can be estimated from data [5]. The former presents the problem that an external DEM may be not available, whereas the later has the handicap that topography estimation is problematic for medium and low coherences [2].

This letter presents a novel interferometric coherence estimation algorithm based on the 2D-DWPT [7], which adapts to the nonhomogeneous natures of both $|\rho|$ and ϕ_x. The necessity to

Manuscript received May 18, 2005; revised July 11, 2005. This work was supported in part by the Spanish CICYT under Grant TIC 2002-04451-C02-01 and in part by the EU-RTN AMPER project under Grant HPRN-CT-2002-00205. The associate editor coordinating the review of this manuscript and approving it for publication was Dr. Antonia Papandreou-Suppappola.

C. López-Martínez and E. Pottier are with the Electronics and Telecommunications Institute of Rennes UMR CNRS 6164, University of Rennes 1, 35042 Rennes Cedex, France (e-mail: carlos.lopez@univ-rennes1.fr; eric.pottier@univ-rennes1.fr).

X. Fàbregas is with the Department of Signal Theory and Communications, Technical University of Catalonia, 08094 Barcelona, Spain (e-mail: fabregas@tsc.upc.edu).

Digital Object Identifier 10.1109/LSP.2005.859513

estimate coherence with a high spatial resolution is important when SAR images reflect areas with man-made structures in order to avoid the mixture and the loss of spatial details. This approach presents three advantages with respect to classical approaches, i.e., (2) and (3). It does not need both SAR images separately to estimate coherence, the estimated coherence is not biased by the topographic phase, and the algorithm allows high spatial resolution coherence estimation.

II. Signal Model and Estimation Algorithm

The measured phase ϕ of the Hermitian product of a pair of SAR images is described by [5]

$$\phi = \phi_x + v \tag{4}$$

where v is a zero-mean noise, independent of ϕ_x, whose variance depends on MN and $|\rho|$ [8]. In [9], it has been demonstrated that the real and imaginary parts of the complex phasor $\exp(j\phi)$ may be described by the noise models

$$\Re\{\exp(j\phi)\} = N_c \cos(\phi_x) + v_c \tag{5}$$
$$\Im\{\exp(j\phi)\} = N_c \sin(\phi_x) + v_s \tag{6}$$

where $\Re\{x\}$ and $\Im\{x\}$ are the real and imaginary parts, respectively, and v_c and v_s are two zero-mean noises with variances equal to

$$\sigma^2_{v_c} = \sigma^2_{v_s} = \frac{1}{2}\left(1 - |\rho|^2\right)^{0.685}. \tag{7}$$

It can be observed that v_c and v_s are independent of ϕ_x. Considering the Gaussian scattering hypothesis [8] to describe ϕ, N_c may be expressed for single look, i.e., nonaveraged, SAR data, as

$$N_c = \int_{-\pi}^{\pi} \cos(v) p_v(v) dv = (\pi/4)|\rho|\, {}_2F_1(1/2, 1/2; 2; |\rho|^2) \tag{8}$$

where $p_v(v)$ is the probability density function of ϕ considering $\phi_x = 0$ [8], and ${}_2F_1(a, b; c; z)$ represents the Gauss hypergeometric function. N_c increases with $|\rho|$, as shown in Fig. 1. Consequently, N_c contains the same information as the original coherence. Equations (5) and (6) allow separating the complex phasor $\exp(j\phi)$ into two components: the additive term $N_c\exp(j\phi_x)$, which contains useful information concerning $|\rho|$ (through the parameter N_c) and the topographic information ϕ_x, and the complex additive noise term $v_c + jv_s$. Hence, if the complex phasor $\exp(j\phi)$ is considered, $|\rho|$ can be obtained if N_c is estimated by using (5) and (6). Thus, it is not necessary to consider both SAR images S_1 and S_2 separately.

III. Wavelet Domain Signal Model

The usefulness of the discrete wavelet transform (DWT) in denoising and estimation problems has been largely demonstrated. Most of the proposed algorithms and techniques are based on hard- or soft-thresholding techniques, which are not considered for the problem described previously. In what follows, we shall perform the 2D-DWPT of $\exp(j\phi)$. If the complex noise component $v_c + jv_s$ is filtered by means of thresholding-like techniques, the topographic phase ϕ_x would not be retrieved correctly. As a result, parameter N_c is not estimated correctly either, presenting a large number of image artifacts. This poor performance has its origin into the fact that, since some complex wavelet coefficients are eliminated, the lack of these coefficients prevents a correct reconstruction of the complex signal $N_c\exp(j\phi_x)$. A new framework to estimate the parameter N_c, adapted to the noise models (5) and (6), is considered next.

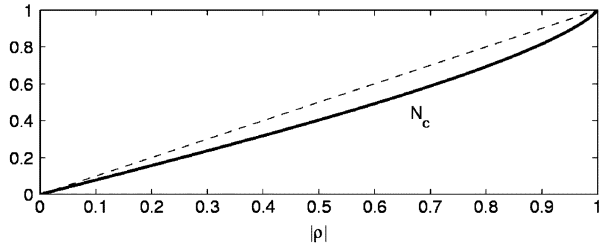

Fig. 1. N_c as a function of $|\rho|$.

If (5) and (6) are considered, the estimation of the coherence by means of N_c is also affected by the bias introduced by the topographic phase component ϕ_x. On the contrary, if one considers the 2D-DWPT of the noise models (5) and (6), by assuming ideal filters, these models translate into the following noise models in the wavelet domain [9]:

$$\mathrm{DWT}_{2D}\{\cos(\phi)\} = 2^i N_c \cos(\phi_x^w) + v_c^w \tag{9}$$
$$\mathrm{DWT}_{2D}\{\sin(\phi)\} = 2^i N_c \sin(\phi_x^w) + v_s^w \tag{10}$$

where i represents the wavelet scale, and ϕ_x^w is a filtered version, in the wavelet domain, of ϕ_x. The term ϕ_x^w corresponds, for each iteration of the 2D-DWPT, to a lowpass and downsampled version for the low-frequency band of the wavelet domain, whereas it is a filtered, downsampled, and frequency-inverted version for the three high-frequency wavelet bands. In (9) and (10), the 2D-DWPT introduces a multiplicative factor equal to 2^i in the first additive term, i.e., the useful information term. Despite the fact that wavelet bands present a two-dimensional bandwidth equal to one fourth of that of the original signal, the 2D-DWPT also introduces a factor 2 (4 when power is considered) that compensates for the bandwidth loss. Consequently, the noise terms in the wavelet domain, i.e., v_c^w and v_s^w, present the same variance values as v_c and v_s. The average wavelet coefficient intensity is obtained, then, as

$$E\{|\mathrm{DWT}_{2D}\exp(j\phi)|^2\} = 2^{2i}N_c^2 + \sigma^2_{v_c^w} + \sigma^2_{v_s^w}. \tag{11}$$

Equation (11) shows that the wavelet transform is able to retrieve coherence information through the parameter N_c, in such a way that the higher the number of wavelet scales, i.e., i, the more negligible the influence of the noise terms. Therefore, for i that is large enough, the wavelet coefficients' intensity is proportional to N_c^2, i.e., proportional to the coherence of the space-frequency area determined by the wavelet coefficient.

As observed in (9) and (10) for ideal wavelet filters, the real and imaginary parts of all coefficients containing useful information are multiplied by 2 for every wavelet scale. This is not the case for real filters, since the band pass is not flat and equal to 2. Thus, the 2D-DWPT must be computed considering wavelet

filters with flat frequency response, achieved by considering filters with a relatively high number of coefficients. The use of short filters decreases the performance of the algorithm, as wavelet coefficients containing useful information are multiplied by values lower than 2, hence preventing their detection.

IV. Coherence Estimation in the Wavelet Domain

In order to estimate N_c, the improving factor 2^i multiplying it, as it is shown in (9) and (10), has to be maintained when the inverse 2D-DWPT is calculated. The proposed algorithm detects, for every wavelet scale that is inversely transformed, those wavelet coefficients containing useful information, i.e., $N_c > 0$, multiplying its real and imaginary parts by 2. The detection is performed by means of

$$\Gamma_{\text{sig}} = \frac{I_w - 2^{2i}\sigma_w^2}{I_w} \tag{12}$$

where I_w is the intensity of the wavelet coefficients, and σ_w^2 [see (7)] is the noise power. This power may be estimated from the intensity of the wavelet coefficients of the high-frequency wavelet scales, since they contain mainly noise [7]. Next, a threshold is applied to (12). The wavelet coefficients presenting Γ_{sig} larger than the threshold are processed, i.e., their real and imaginary parts are multiplied by 2, whereas those below it are maintained, avoiding introducing false information. The final effect of this process is that the weight of those wavelet coefficients classified as coefficients containing useful information is increased with respect to those coefficients that are not processed. Thus, the influence of the noise terms v_c and v_s is reduced with respect to N_c. Once the inverse 2D-DWPT is applied to the processed signal, the derived complex phasor in the original domain presents an amplitude proportional to N_c and a denoised topographic phase [9]. In order to derive the coherence information, denoted as $|\rho_{\text{WLT}}|$ in the following, the amplitude may be normalized by $2^{i_{\max}}$, where $i_{\max}$ represents the maximum number of scales of the 2D-DWPT. The selection of the number of wavelets scales $i_{\max}$ is, in principle, arbitrary. Nevertheless, if the number of wavelet scales is increased too much, the wavelet coefficients in the low-frequency scales will mask those coefficients in the high-frequency scales. This effect will result in a loss of spatial resolution in the coherence image. Finally, (8) is employed to invert N_c in order to derive $|\rho_{\text{WLT}}|$.

V. Results

First, two phase ramps have been simulated over the complete coherence range. The first interferogram presents a 2π phase excursion, i.e., a phase fringe, over 40 pixels. The second has a 12-pixel fringe. In both cases, $|\rho_{\text{MLT}}|$ and $|\rho_{\text{PHC}}|$ have been calculated with a 5×5 analysis window (see Fig. 2). For the 40-pixel fringe phase, both approaches estimate the correct $|\rho|$ values, as ϕ_x is basically constant within the averaging window. For the 12-pixel fringe interferogram, the estimator $|\rho_{\text{MLT}}|$ presents a clear bias since ϕ_x cannot be considered constant over the averaging window. Nevertheless, $|\rho_{\text{PHC}}|$ estimates the correct $|\rho|$ since ϕ_x is compensated for. Finally, if $|\rho_{\text{WLT}}|$ is applied to both cases (in a four-iteration 2D-DWPT configuration with 40 coefficient Daubechies filters [7]), nonbiased $|\rho|$ values are retrieved without compensation of the topographic

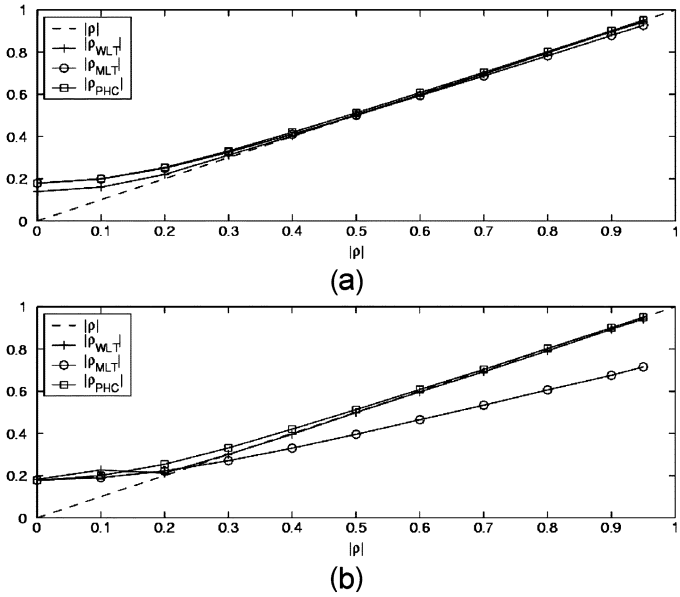

Fig. 2. Estimated coherences for simulated data. (a) Forty-pixel fringe interferogram. (b) Twelve-pixel fringe interferogram.

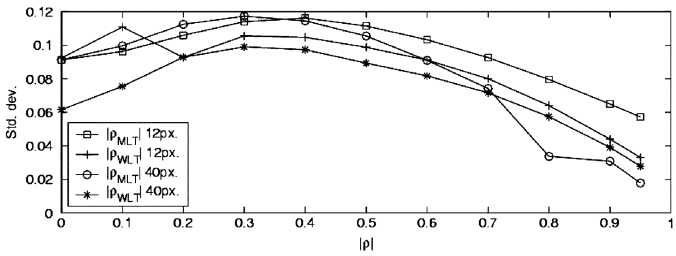

Fig. 3. Coherence estimators' standard deviation for simulated data.

term ϕ_x, since the 2D-DWPT allows to decouple the estimation of the $|\rho|$ from the random phase term v. As deduced in [2] and [9], a speckle-induced bias is observed for low coherences. In the case of $|\rho_{\text{MLT}}|$, this bias term decreases if the number of averaged pixels is increased but at the cost of losing spatial details. In the case of $|\rho_{\text{WLT}}|$, this bias decreases by increasing the maximum number of wavelets scales $i_{\max}$, which cannot be increased arbitrarily, as indicated previously. Nevertheless, the properties of the 2D-DWPT allow minimizing the spatial resolution losses with respect to multilook techniques. Fig. 3 presents the standard deviation measurements for $|\rho_{\text{MLT}}|$ and $|\rho_{\text{WLT}}|$.

The estimators $|\rho_{\text{MLT}}|$ (within a 5×5 pixel analysis window) and $|\rho_{\text{WLT}}|$ (in a three-iteration 2D-DWPT configuration with 40 coefficient Daubechies [7]) are also applied to an ESAR-DLR X-band interferogram of Mt. Etna (Italy), representing steep slopes (see Fig. 4). As presented by Fig. 4(c), the image difference $|\rho_{\text{WLT}}| - |\rho_{\text{MLT}}|$ shows a bias, which is highly noticeable in the steepest slopes and located at the center of the image. Nevertheless, if ϕ_x is estimated from the data, the image difference $|\rho_{\text{WLT}}| - |\rho_{\text{PHC}}|$ does not show bias [see Fig. 4(d)]. A wavelet technique is employed to estimate ϕ_x [9]. Table I presents the average value of the difference images in the areas selected in Fig. 4(c) and (d). In area A, it is observed that $|\rho_{\text{WLT}}|$ is able to reduce a small bias. The proposed approach estimates coherence without a bias also

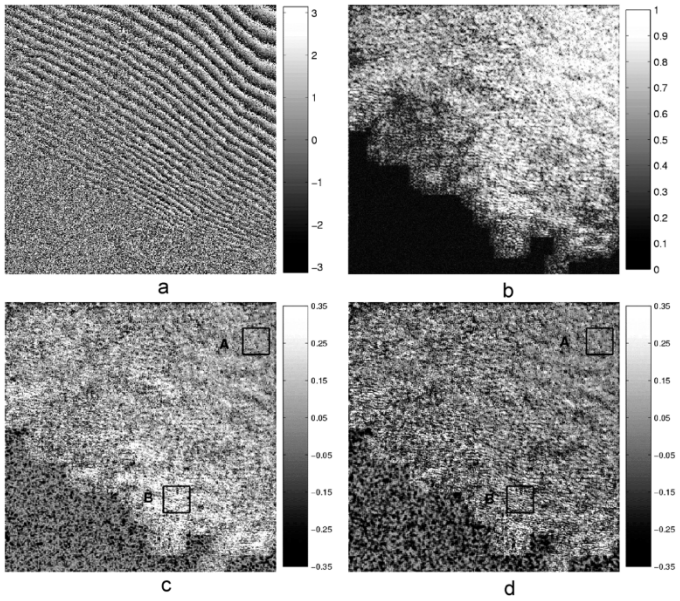

Fig. 4. (a) ESAR-DLR X-band Mt. Etna interferometric phase. (b) ESAR-DLR Mt. Etna interferometric coherence $|\rho_{\mathrm{WLT}}|$. (c) Difference image $|\rho_{\mathrm{WLT}}| - |\rho_{\mathrm{MLT}}|$. (d) Difference image $|\rho_{\mathrm{WLT}}| - |\rho_{\mathrm{PHC}}|$.

TABLE I
DIFFERENCE IMAGES AVERAGE VALUES

	$\widehat{\lvert\rho_{WLT}\rvert - \lvert\rho_{MLT}\rvert}$	$\widehat{\lvert\rho_{WLT}\rvert - \lvert\rho_{PHC}\rvert}$
Zone A	0.050	0.004
Zone B	0.160	-0.007

in steep slopes areas, as observed in area B. Hence, $|\rho_{\mathrm{WLT}}|$ estimates coherence without a bias respect to ϕ_x. As shown, the algorithm estimates a correct coherence in the case of steep slopes. Nevertheless, this estimation may be problematic for highly steep slopes. In this case, useful information appears in the first wavelet scales. Considering (9) and (10), one can observe that the real and imaginary parts of those wavelet coefficients containing useful information are only multiplied by 2. The limited increase of amplitude due to the 2D-DWPT can provoke that low-coherence values may not be estimated correctly since the amplitude of the wavelet coefficients is mainly due to noise. Nevertheless, high coherences may be estimated correctly since they are basically proportional to $2N_c$ [see (11)].

The 2D-DWPT was selected to exploit its capability to perform high spatial resolution coherence estimation [7]. To present this property, an ESAR-DLR L-band interferogram of the Oberfapfenhoffen test site (Germany) is considered. The area is characterized by a flat topography that does not bias coherence estimation. Nevertheless, it contains man-made structures which spatial resolution must be maintained. Fig. 5(a) corresponds to $|\rho_{\mathrm{MLT}}|$, whereas Fig. 5(b) corresponds to $|\rho_{\mathrm{WLT}}|$. The horizontal lines correspond to a parking lot. In this area, high coherence values are expected for the cars due to their metallic nature, whereas low values are expected for the lanes separating them. The lanes are dominated by specular reflection; hence, they contain mainly uncorrelated additive noise. Fig. 5(c) presents the profiles of $|\rho_{\mathrm{MLT}}|$ and $|\rho_{\mathrm{WLT}}|$. The profile corresponding to the image S_1 is also included but

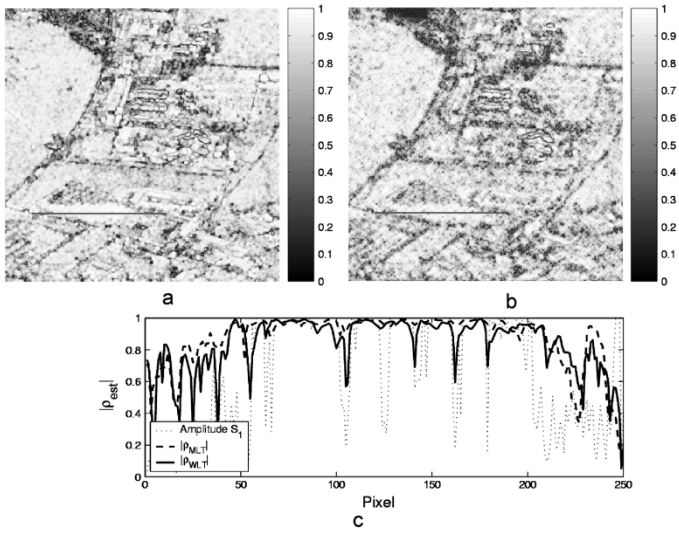

Fig. 5. ESAR-DLR L-band SAR interferometric dataset. (a) $|\rho_{\mathrm{MLT}}|$. (b) $|\rho_{\mathrm{WLT}}|$. (c) Images profiles.

conveniently scaled. In the profile of S_1, the separation lanes between the parked cars are visible. Due to the spatial averaging, these lanes disappear in $|\rho_{\mathrm{MLT}}|$, whereas they become visible for $|\rho_{\mathrm{WLT}}|$.

VI. CONCLUSION

A novel InSAR high spatial resolution coherence estimator based on the 2D-DWPT, significantly departing from classical thresholding-like techniques, is presented. As it is shown, the properties of the 2D-DWPT allow separating coherence estimation from the phase component, which results in a coherence estimation process not affected by topographic biases. In addition, the high spatial resolution capabilities of the 2D-DWPT allow increasing the amount of information contained in the coherence parameter.

REFERENCES

[1] R. Bamler and P. Hartl, "Synthetic aperture radar interferometry," *Inverse Problems*, vol. 14, pp. R1–R54, 1998.
[2] R. Touzi, A. Lopes, J. Bruniquel, and P. W. Vachon, "Coherence estimation for SAR imagery," *IEEE Trans. Geosci. Remote Sens.*, vol. 37, no. 1, pp. 135–149, Jan. 1999.
[3] S. R. Cloude and K. P. Papathanassiou, "Polarimetric SAR interferometry," *IEEE Trans. Geosci. Remote Sens.*, vol. 36, no. 5, pp. 1551–1565, Sep. 1998.
[4] F. Gatelli, A. M. Guarnieri, F. Parizzi, P. Pasquali, C. Prati, and F. Rocca, "The wavenumber shift in SAR interferometry," *IEEE Trans. Geosci. Remote Sens.*, vol. 32, no. 4, pp. 855–865, Jul. 1994.
[5] J. S. Lee, K. P. Papathanassiou, T. L. Ainsworth, M. R. Grunes, and A. Reigber, "A new technique for noise filtering of SAR interferometric phase images," *IEEE Trans. Geosci. Remote Sens.*, vol. 36, no. 5, pp. 1456–1465, Sep. 1998.
[6] A. M. Guarnieri and C. Prati, "SAR interferometry: A quick and dirty coherence estimator for data browsing," *IEEE Trans. Geosci. Remote Sens.*, vol. 35, no. 3, pp. 660–669, May 1997.
[7] S. Mallat, *A Wavelet Tour of Signal Processing*, 2nd ed. San Diego, CA: Academic, 1998.
[8] J. S. Lee, K. W. Hoppel, S. A. Mango, and A. R. Miller, "Intensity and phase statistics of multilook polarimetric interferometric SAR imagery," *IEEE Trans. Geosci. Remote Sens.*, vol. 32, no. 5, pp. 1017–1028, Sep. 1994.
[9] C. López-Martínez and X. Fábregas, "Modeling and reduction of SAR interferometric phase noise in the wavelet domain," *IEEE Trans. Geosci. Remote Sens.*, vol. 40, no. 12, pp. 2553–2566, Dec. 2002.